

# SNR Comparisons of Beamforming Strategies

Jie Liu, Kang-Sik Kim, and Michael F. Insana, *Senior Member, IEEE*

**Abstract**—This paper defines the echo signal-to-noise ratio (eSNR) for pulse-echo systems that adapts to the effects of shift-varying impulse responses, spatiotemporal coding, and various beamformers. Measurement techniques using point targets or random scattering media can be interrelated for a broad range of experimental conditions through the eSNR. The eSNR definitions are also illustrated by comparing a spatial matched filter (SMF) beamformer to conventional dynamic receive focusing methods to evaluate performance based on resolution and sensitivity. Closed-form expressions are presented that predict eSNR gains from SMF approaches relative to other beamformers.

## I. INTRODUCTION

IN many ways, beamformers are the most important component of ultrasound systems. The goal of beamformers is to create uniformly narrow beams with low sidelobe amplitude over as long a depth as possible [1]. Evaluation of beamforming strategies requires consideration of relative image quality, cost, and speed. We and others found that spatial filtering can focus acoustic beams with acceptable image quality at low cost but with some loss of frame rate [2]–[4]. For example, the echo signal-to-noise ratio (eSNR) improves in the near field when spatial matched filters are applied to fixed-point-focus echo data as compared with traditional dynamic receive focusing (DRF) [5], [6]. However, the degree of improvement depends on how eSNR is defined, and there are numerous definitions in the literature [7], [8]. An eSNR is a scalar quantity frequently used to assess detection sensitivity. It is an important element of system dynamic range that helps determine contrast resolution for the imaging system. Despite its importance and widespread use, there is no consistent definition that applies across research applications.

This paper gives a general expression of the eSNR for shift-variant B-mode imaging, describes an analytical method for computing eSNR enhancement from spatial matched filtering and spatiotemporal matched filtering beamformers, and verifies predictions using Field II simulation [9] and phantom measurements. Several beamforming strategies are compared in terms of eSNR in Section V, including fixed focusing, dynamic receive focusing (DRF), spatial matched filtering (SMF) on beamformed data, spatial match filtering of individual array elements [4], and spatiotemporal filtering (STF) [6].

Manuscript received September 6, 2006; accepted January 4, 2007.

The authors are with the Department of Bioengineering, University of Illinois at Urbana-Champaign, Urbana, IL 61801 (e-mail: mfi@uiuc.edu).

Digital Object Identifier 10.1109/TUFFC.2007.346

## II. ECHO SIGNAL MODEL

A linear equation describing time-varying, pulse-echo RF signals  $g(\mathbf{t})$  in terms of the spatial distribution of an object function<sup>1</sup>  $f(\mathbf{x}, t')$  over the region of support  $\Omega$  and with the spatiotemporal impulse response  $h(\mathbf{x}, \mathbf{t})$  is [10]–[12]

$$g(\mathbf{t}) = s(\mathbf{t}) + e(\mathbf{t}),$$

$$\text{where } s(\mathbf{t}) = \int_{\Omega} d\mathbf{x} h(\mathbf{x}, \mathbf{t}) f(\mathbf{x}, t'). \quad (1)$$

Here,  $s(\mathbf{t})$  is the signal and  $e(\mathbf{t})$  the signal-independent noise;  $\mathbf{x} = (x_1, x_2, x_3)$  is the three-dimensional (3-D) position vector in the object relative to the transducer surface, and  $\mathbf{t} = (t_1, t_2)$  is the 2-D time vector for echo data acquisition corresponding to one image frame;  $t_1 = \ell T$ ,  $0 \leq \ell \leq L - 1$ , describes the  $L$  range samples recorded on the sampling interval  $T$  for one A-line in the RF frame, and  $t_2 = mLT$ ,  $0 \leq m \leq M - 1$ , identifies the  $M$  sequential A-lines recorded in a frame. The acquisition time is given by  $t' = t_1 + t_2 = (\ell + mL)T$ . Eq. (1) may be expressed as a continuous-to-discrete transformation

$$g[\ell, m] = s[\ell, m] + e[\ell, m]$$

$$= \int_{\Omega} d\mathbf{x} h(\mathbf{x}, [\ell, m]) f(\mathbf{x}, t') + e[\ell, m]. \quad (2)$$

For stationary scatterers,  $f(\mathbf{x}, t') = f(\mathbf{x})$ , (2) describes objects entirely in terms of their spatial position and reflectivity. Signals are described entirely in terms of acquisition time  $t'[\ell, m]$  and voltage amplitude. Nevertheless,  $\ell$  can be related to depth along the beam axis  $x_1$  for sound speed  $c$  via  $\ell = 2x_1/cT$ , and  $m$  is related to lateral position  $x_2$  via  $m = x_2/\Delta x_2$ , where  $\Delta x_2$  is the lateral scan interval. Simulation of echo signals requires that continuous object functions be sampled, which yields the object vector  $\mathbf{f}$  through lexicographical reordering. Consequently, (2) can also be expressed in compact matrix form,  $\mathbf{g} = \mathbf{H}\mathbf{f} + \mathbf{e}$ .

The B-mode image displays an estimate of the object function in the scan plane,  $\hat{\mathbf{f}} = \hat{f}(x_1, x_2)$ . Image data are found by applying a nonlinear operator to the RF echo frame,  $\hat{\mathbf{f}} = \mathcal{O}\mathbf{g}$ , that includes envelope detection, low-pass filtering, logarithmic amplitude compression, and scan conversion [12]. The eSNR discussion below is limited to the RF signal,  $\mathbf{g}$ . Discussions of B-mode speckle statistics may be found elsewhere, e.g., [13].

<sup>1</sup>The term  $f(\mathbf{x}, t')$  is related to the acoustic impedance  $\xi$  through the relation  $f(\mathbf{x}, t') = \mathcal{F}_t^{-1}\{\xi(\mathbf{x})\omega^2/c^2\}$ , where  $\mathcal{F}_t^{-1}$  is the inverse temporal Fourier transform operator,  $t'$  is echo acquisition time,  $\omega$  is radial frequency, and  $c$  is sound speed.

If  $\mathbf{f}$  is stochastic and the object and noise functions are each zero-mean multivariate normal (MVN), we have

$$\mathbf{f} \sim \text{MVN}(\mathbf{0}, \sigma_f^2 \mathbf{I}) \quad \text{and} \quad \mathbf{e} \sim \text{MVN}(\mathbf{0}, \sigma_e^2 \mathbf{I}). \quad (3)$$

The covariance matrices for independent samples are products of variance,  $\sigma_f^2$  or  $\sigma_e^2$ , and the identity matrix  $\mathbf{I}$ .

### III. eSNR DEFINITIONS

A common general definition of SNR [7] is the ratio of signal energy to noise energy within the time interval of the acquisition frame,  $T' = MLT$ . The eSNR for beamformed RF ultrasonic data may be written as

$$\text{eSNR} = \frac{\mathcal{E} \left\{ \sum_{\ell, m} [\mathcal{E}\{g[\ell, m]\}_{e|f}]^2 \right\}_f}{\mathcal{E} \left\{ \sum_{\ell, m} e^2[\ell, m] \right\}_e}, \quad (4)$$

The notation  $\mathcal{E}\{\mathbf{g}\}_{e|f}$  denotes ensemble average of the echo frame  $\mathbf{g}$  over the noise process  $e$  for a fixed realization of the stochastic object  $f$ . In the following, we shift the image plane axis to the center of the image,  $-L/2 \leq \ell \leq L/2 - 1$ ,  $-M/2 \leq m \leq M/2 - 1$ .

#### A. Random Scattering Media

Applying (2)–(4) to random scattering media under the ergodic assumption, and noting that  $\mathcal{E}\{\mathbf{g}\}_{e|f} = \mathbf{H}\mathbf{f}$  and  $\mathcal{E}\{f(\mathbf{x})f(\mathbf{x}')\}_f = \sigma_f^2 \delta(\mathbf{x} - \mathbf{x}')$  (scattering intensity per volume), we find

$$\begin{aligned} \text{eSNR}_r &= \frac{\sum_{\ell, m} \int_{\Omega} d\mathbf{x} \int_{\Omega} d\mathbf{x}' h(\mathbf{x}, [\ell, m]) h(\mathbf{x}', [\ell, m]) \mathcal{E}\{f(\mathbf{x})f(\mathbf{x}')\}}{\sum_{\ell, m} \mathcal{E}\{e^2[\ell, m]\}} \\ &= \frac{\sigma_f^2}{\sigma_e^2 LM} \sum_{\ell, m} \int_{\Omega} d\mathbf{x} h^2(\mathbf{x}, [\ell, m]) \\ &= \frac{\sigma_f^2}{\sigma_e^2} \left( \frac{1}{LM} \sum_{\ell, m} E_h \right) = \frac{\sigma_f^2 \langle E_h \rangle}{\sigma_e^2}. \end{aligned} \quad (5)$$

The denominator in the first form of (5) was reduced to  $\sigma_e^2 LM$ . The spatial integral in the second form is interpreted as the energy from the pulse,  $E_h$ , available to each measurement sample,  $g[\ell, m]$ . The final form shows us the ratio of echo signal energy to noise energy, where the reflectivity of scatterers is described by  $\sigma_f^2$  and the time-averaged energy of the pulse is  $\langle E_h \rangle$ .

Ignoring the physical order of the signal formation process, we can invert the order of the sum and integral in (5) to find

$$\begin{aligned} \text{eSNR}_r &= \frac{\sigma_f^2}{\sigma_e^2} \int_{\Omega} d\mathbf{x} \left( \frac{1}{LM} \sum_{\ell, m} h^2(\mathbf{x}, [\ell, m]) \right) \\ &= \frac{\sigma_f^2}{\sigma_e^2} \int_{\Omega} d\mathbf{x} \phi_h(\mathbf{x}, \mathbf{0}). \end{aligned} \quad (6)$$

The term  $\phi_h(\mathbf{x}, \mathbf{0})$  is the deterministic autocorrelation function of  $h$  over time at zero lag. It may be interpreted as an average sensitivity in the scan plane to scatterers positioned at different points in region  $\Omega$ . In (5) and (6), the  $\text{eSNR}_r$  is unitless, scalar valued, and proportional to the ratio of object and noise variances. If  $h$  does not vary with position, then (6) gives  $\int_{\Omega} d\mathbf{x} \phi_h(\mathbf{x}, \mathbf{0}) = \phi_h(\mathbf{0}) \int_{\Omega} d\mathbf{x} = \phi_h'(\mathbf{0})$ , which we know from (5) is just the average pulse energy  $\langle E_h \rangle$  but written as the product of temporal correlation and volume. The shift-invariant result is

$$\text{eSNR}_r = \frac{\sigma_f^2}{\sigma_e^2} \phi_h'(\mathbf{0}). \quad (7)$$

#### B. Single Point Scatterer

It can be more convenient to measure signals from a “point target” than from a random scattering medium, provided the results can be related. Assume a single point scatterer of reflective amplitude  $A$  is located at  $\mathbf{x}$  for all  $t'$  so that  $f(\mathbf{x}, t') = A\delta(\mathbf{x}' - \mathbf{x})$ . From (4), the eSNR for a point scatterer is

$$\text{eSNR}_p(\mathbf{x}) = \frac{A^2}{\sigma_e^2} \phi_h(\mathbf{x}, \mathbf{0}), \quad (8)$$

showing that, of course, the echo signal-to-noise ratio for a point target can vary with scatterer position. Combining (5) and (8) gives the comparative relationship

$$\text{eSNR}_r = \frac{\sigma_f^2}{A^2} \int_{\Omega} d\mathbf{x} \text{eSNR}_p(\mathbf{x}), \quad (9)$$

which, for shift-invariant systems, yields

$$\text{eSNR}'_p = \text{eSNR}_p \int_{\Omega} d\mathbf{x} \quad \text{and} \quad \text{eSNR}_r = \frac{\sigma_f^2}{A^2} \text{eSNR}'_p. \quad (10)$$

Eqs. (9) and (10) show that the eSNR from a random medium is proportional to the ratio of random scatterer strength per volume of medium  $\sigma_f^2$  and the scattering intensity of the point reflector  $A^2$ . It is also proportional to the eSNR for point reflectors integrated over the scattering volume  $\Omega$ . Note that factors describing ultrasonic attenuation and time-gain compensation may be combined with  $h(\mathbf{x}, t')$  and thus included as components of a shift-varying system response.

### IV. BEAMFORMING WITH SPATIOTEMPORAL FILTERS

“Spatial filtering” is a term often applied to processing of RF echo data  $\mathbf{g}$  to facilitate beamforming in the process

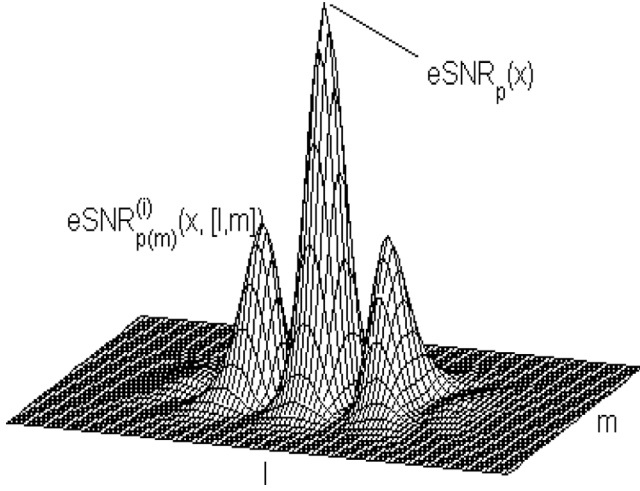


Fig. 1. Illustration of the  $eSNR_{p(m)}^{(i)}$  over the received echo plane  $[\ell, m]$ .

of forming image  $\hat{\mathbf{f}}$  [14]. It is thought of as spatial filtering because the effects are observed in the image, but in fact a 2-D temporal filter is applied to RF data. We reserve the term “temporal filtering” to refer to compression of coded pulses [15], and “spatiotemporal filtering” (STF) as a combination of these two methods [6].

#### A. Spatial Filtering

Applying  $w[\ell, m]$  to echo data  $g[\ell, m]$ , we obtain the filtered echo signal

$$g_w[\ell, m] = \sum_{\ell', m'} w[\ell - \ell', m - m'] g[\ell', m']. \quad (11)$$

The spatial matched filter (SMF),  $w[\ell, m] = h(\mathbf{x}, [-\ell, -m])$ , is one example of a beamforming filter able to focus more of the pulse energy than dynamic receive focusing, and has been shown to provide a greater  $eSNR_p$  [4]. For a point target and matched-filter processing, (4) and (11) yield

$$\begin{aligned} eSNR_{p(m)}(\mathbf{x}) &= \frac{A^2 \sum_{\ell, m} \phi_h^2(\mathbf{x}, [\ell, m])}{\sigma_e^2 \phi_h(\mathbf{x}, [0, 0])} \\ &= \sum_{\ell, m} \left[ \frac{A^2 \phi_h^2(\mathbf{x}, [\ell, m])}{\sigma_e^2 \phi_h(\mathbf{x}, [0, 0])} \right] \\ &= \sum_{\ell, m} eSNR_{p(m)}^{(i)}(\mathbf{x}, [\ell, m]). \end{aligned} \quad (12)$$

The  $eSNR_{p(m)}(\mathbf{x})$  is the echo signal-to-noise ratio from a point reflector using an SMF beamformer. It is an integration of instantaneous values,  $eSNR_{p(m)}^{(i)}$ , that are illustrated in Fig. 1 for a 10-MHz linear array transducer with 80% bandwidth and focused at  $\mathbf{x} = (x_1, 0, 0) = 40$  mm. These results were simulated using Field II. The maximum value for the  $eSNR_{p(m)}^{(i)}$  is located at  $\ell = 0, m = 0$  and is equal to  $eSNR_p(\mathbf{x})$  from (8).

Interestingly, the  $eSNR_{p(m)}^{(i)}$  is monotonic with the “spatial resolution cell” concept widely used (see Eq. (31) in [16]). Eq. (12) and Fig. 1 show that the  $eSNR_{p(m)}^{(i)}$  describes the sensitivity of the system to different points in the medium, which is a spatial resolution metric. The eSNR and spatial resolution can be closely related. Methods that improve the eSNR by widening the distribution of the  $eSNR_{p(m)}^{(i)}$ , e.g., by increasing the pulse length when the time-bandwidth product (TBP) is one, do so at the expense of spatial resolution. However, methods that scale the amplitude of the  $eSNR_{p(m)}^{(i)}$  without widening the distribution, e.g., varying f-number or output power, influence the eSNR independent of spatial resolution. The summation over temporal samples in (12) provides a scalar measure at point-scatterer position  $\mathbf{x}$  but also discards spatial resolution information.

The gain from SMF beamforming relative to fixed-focus methods is found from the ratio

$$\begin{aligned} \gamma_{p(m)}(\mathbf{x}) &= \frac{eSNR_{p(m)}(\mathbf{x})}{eSNR_p(\mathbf{x})} \\ &= \frac{\sum_{\ell, m} \phi_h^2(\mathbf{x}, [\ell, m])}{\phi_h^2(\mathbf{x}, [0, 0])} \\ &= 1 + \frac{\sum_{\ell, m \neq 0} \phi_h^2(\mathbf{x}, [\ell, m])}{\phi_h^2(\mathbf{x}, [0, 0])}. \end{aligned} \quad (13)$$

Since  $\phi_h^2(\mathbf{x}, [\ell, m])$  is positive semidefinite,  $\gamma_{p(m)} \geq 1$ ; i.e., matched filtering improves the eSNR. Equality is approached as the pulse bandwidth (in the 2-D sense described below) increases and  $\phi_h^2(\mathbf{x}, [\ell, m]) \rightarrow \phi_h^2(\mathbf{x}, [0, 0])\delta[\ell, m]$ .

For random scattering media and matched-filter processing, (9) yields

$$eSNR_{r(m)} = \frac{\sigma_f^2}{A^2} \int_{\Omega} d\mathbf{x} eSNR_{p(m)}(\mathbf{x}), \quad (14)$$

and the corresponding eSNR gain for region  $\Omega$  is

$$\gamma_{r(m)\Omega} = \frac{\int_{\Omega} d\mathbf{x} eSNR_{p(m)}(\mathbf{x})}{\int_{\Omega} d\mathbf{x} eSNR_p(\mathbf{x})} \geq \min \gamma_{p(m)}(\mathbf{x}). \quad (15)$$

Eq. (15) shows that the eSNR gain for random media is at least as large as that estimated from a point target. The exact value depends on details of the beam properties and may be found numerically.

The above analysis gives the eSNR gain for an SMF applied to beamformed RF signals; that is, echo signals that are filtered after receive-channel summation. Alternatively, an SMF can be applied to signals from individual receive channels before summation. The latter approach generates relatively lower sidelobe amplitudes and higher lateral resolution [4], although computational loads increase significantly. The echo signal of a point scatterer located at  $\mathbf{x}_0$  received on the  $i$ -th channel of an  $N$ -element array is

$$g_i[\ell, m] = s_i[\ell, m]_{\mathbf{x}_0} + e_i[\ell, m], \quad i = 1, 2, \dots, N, \quad (16)$$

where  $s_i[\ell, m]_{\mathbf{x}_0} = Ah_i(\mathbf{x}, [\ell, m])$  and the noise per channel is  $\mathbf{e}_i \sim \text{MVN}(\mathbf{0}, (\sigma_e^2/\mathbf{N})\mathbf{I})$ . Assuming we have a fixed transmit/receive focal length, the beamformed RF echo signal is the summation without time delay,

$$s[\ell, m]_{\mathbf{x}_0} = \sum_{i=1}^N Ah_i(\mathbf{x}, [\ell, m]).$$

Spatial matched filtering the beamformed echo signal yields

$$\begin{aligned} \mathcal{E}\{g_w[\ell, m]\}_e &= A^2 \phi_h(\mathbf{x}, [\ell, m]) \\ &= A^2 \sum_i \phi_{h_i}(\mathbf{x}, [\ell, m]) + A^2 \sum_{i \neq j} \phi_{h_{ij}}(\mathbf{x}, [\ell, m]) \\ &\triangleq A^2 [Q_1(\mathbf{x}, [\ell, m]) + Q_2(\mathbf{x}, [\ell, m])], \end{aligned} \quad (17)$$

and substituting (17) into (12) gives

$$\text{eSNR}_{p(m)}(\mathbf{x}) = \frac{A^2 \sum_{\ell, m} [Q_1(\mathbf{x}, [\ell, m]) + Q_2(\mathbf{x}, [\ell, m])]^2}{\sigma_e^2 [Q_1(\mathbf{x}, [0, 0]) + Q_2(\mathbf{x}, [0, 0])]}. \quad (18)$$

Conversely, if the receive-channel echoes are filtered individually before summation (ESMF), the signal is given by

$$\mathcal{E}\{g_w[\ell, m]\}_e = A^2 \sum_{i=1}^N \phi_{h_i}(\mathbf{x}, [\ell, m]). \quad (19)$$

The eSNR for the ESMF beamformer is

$$\text{eSNR}_{ep(m)}(\mathbf{x}) = \frac{A^2 N \sum_{\ell, m} Q_1^2(\mathbf{x}, [\ell, m])}{\sigma_e^2 [Q_1(\mathbf{x}, [0, 0])]}. \quad (20)$$

Eqs. (19) and (20) show that filtering echoes before summation eliminates the cross terms  $Q_2$  found in (17) and (18) that generate acoustic sidelobes. Consequently, an ESMF has better contrast resolution than an SMF. The eSNR gain comparisons for the two methods are provided in Section V.

### B. Temporal and Spatiotemporal Filtering

Coded voltage waveforms  $c[\ell]$  have a high time-bandwidth product ( $\text{TBP} > 1$ ) and desirable properties regarding orthogonality [17]. The echo signal from a coded transmission is found from (2) by convolution with the discrete-time code  $c$ ,

$$g'[\ell, m] = \int_{\Omega} d\mathbf{x} \left( \sum_{\ell'} c[\ell - \ell'] h(\mathbf{x}, [\ell', m]) \right) f(\mathbf{x}) + e[\ell, m]. \quad (21)$$

Echo signals can be decoded to recover axial resolution (pulse compression) in different ways. For example, matched filtering  $g'$  with  $c[-\ell]$  yields

$$\begin{aligned} g_t[\ell, m] &= \sum_{\ell'} c[\ell + \ell'] g'[\ell', m] \\ &= \sum_{\ell'} \phi_c[\ell - \ell'] \int_{\Omega} d\mathbf{x} h(\mathbf{x}, [\ell', m]) f(\mathbf{x}) \\ &\quad + \sum_{\ell'} c[\ell + \ell'] e[\ell', m] \\ &\simeq K s[\ell, m] + e_c[\ell, m]. \end{aligned} \quad (22)$$

The last form of (22) assumes ideal conditions where the pulse is completely compressed such that  $s$  is recovered, i.e.,  $\phi_c[\ell] \simeq K\delta[\ell]$ , so the echo signal amplitude is increased by the factor  $K$  equal to the TBP of the coded waveform [15]. The term  $e_c[\ell, m]$  is filtered noise.

It is easy to show [15] that the eSNR gain from temporal filtering of coded pulses is  $\gamma_{p(t)}(\mathbf{x}) = \text{eSNR}_{p(t)}(\mathbf{x})/\text{eSNR}_p(\mathbf{x}) = K$ . From (15), the combined gain from spatiotemporal filtering (STF) is

$$\gamma_{r(m,t)\Omega} = \gamma_{r(t)\Omega} \times \gamma_{r(m)\Omega} = K \frac{\int_{\Omega} d\mathbf{x} \text{eSNR}_{p(m)}(\mathbf{x})}{\int_{\Omega} d\mathbf{x} \text{eSNR}_p(\mathbf{x})}. \quad (23)$$

## V. RESULTS

The derivations and predictions above are validated using Field II simulations and measurements on a Siemens Antares system (Siemens Medical Systems, Issaquah, WA) with a linear array transducer. The center frequency of the transmitted pulse is 10 MHz and the  $-6$  dB fractional bandwidth 55%. The array element pitch is 0.10 mm. In all situations, the transmit focus is 40 mm; the receive and elevational foci are set at 40 mm except were stated otherwise. The number of transmit-receive channels is fixed at 96 (no aperture growth). The frequency-dependent attenuation is 0.5 dB/cm/MHz and the speed of sound is 1540 m/s.

Shift-varying point spread functions were generated by moving a point reflector from 15 mm to 64 mm along the depth and  $\pm 6$  mm laterally [Fig. 2(a)]. The  $\text{eSNR}_p(\mathbf{x})$  was estimated from a point target at each point on the grid using (8) and is expressed in decibels. We also generated echo signals from random scattering media [Fig. 2(b)] in a 5 mm  $\times$  5 mm region centered at 20-, 40-, and 60-mm depths to represent the near field, focal zone, and far field, respectively, of the fixed 40-mm focal length.

### A. The $\text{eSNR}_p(\mathbf{x})$ and the $\text{eSNR}_r$

Eq. (9) allows us to predict the eSNR of a random scattering medium from that of a point reflector, and (6) enables us to compute the  $\text{eSNR}_r$  directly from the echo data  $\mathbf{g}$ . Both are compared below. The random object function  $\mathbf{f}$  was generated numerically in two-dimensional using Monte Carlo methods [18] and “scanned” via (2) before adding noise. An example of a 5 mm  $\times$  5 mm region is given in Fig. 2(b).

The point spread function (psf) shape changes with depth and also laterally near the edge of the transducer.

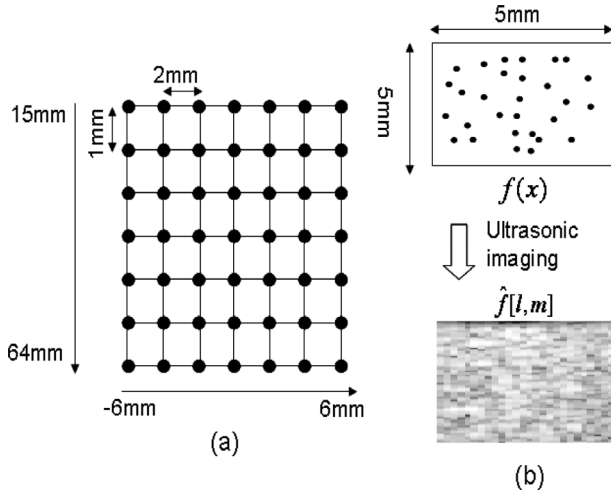


Fig. 2. (a) Shift-varying point-spread functions are estimated on a grid; (b) random scatterers (top) are imaged to generate the simulated echo field (bottom).

The width of the transducer is 19.2 mm, covering the region laterally from  $-9.6$  mm to  $9.6$  mm. The psfs are laterally shift invariant in the selected region ( $-6$  mm to  $6$  mm). For the parameters used in this study, the  $eSNR_p(\mathbf{x})$  was found to be a smoothly varying function of position. We found the correlation coefficient between two psfs placed 1 mm apart in depth is  $> 0.97$ . Consequently, we felt confident interpolating these psf results to a finer mesh grid. Results were upsampled using a bilinear interpolation factor of 200 to refine the grid to  $0.01$  mm  $\times$   $0.01$  mm. The  $eSNR_p$  value of the nearest point on the grid was assigned to each scatterer in the region.

The  $eSNR_r$  was computed from the  $eSNR_p$  to find the values 55.29, 42.23, and 11.08 dB from regions centered at depths 20, 40, and 60 mm, respectively. Values of the  $eSNR_r$  estimated directly from the simulated echo data were 55.30, 42.21, and 10.96 dB, respectively. The equality of results verifies the linear relationship between the  $eSNR_p$  and the  $eSNR_r$  from (9). The data also suggest that point target estimates can be used to accurately predict the eSNR from random media provided the scattering amplitudes are known.

For shift-invariant situations, (10) gives  $eSNR_r/eSNR_p = (\sigma_f^2 \int_{\Omega} d\mathbf{x})/A^2$ , suggesting that the ratio should increase with the volume of the medium. The volume is projected to an area in a 2-D image. This prediction was tested experimentally using a spatially uniform graphite-gelatin phantom scanned with a Siemens Antares system. The volume depth was limited to 1 mm so that the mean scattering amplitude remained wide-sense stationary throughout the field. Fig. 3 shows that the ratio  $eSNR_r/eSNR_p$  increases in proportion during scanning while the scattering volume is being widened.

### B. The eSNR Gain for SMF and DRF Beamformers

A Field II simulation study was conducted to verify the predictions of eSNR gain for spatial matched filtering. The gain, (13), depends on the shape of the autocorrelation

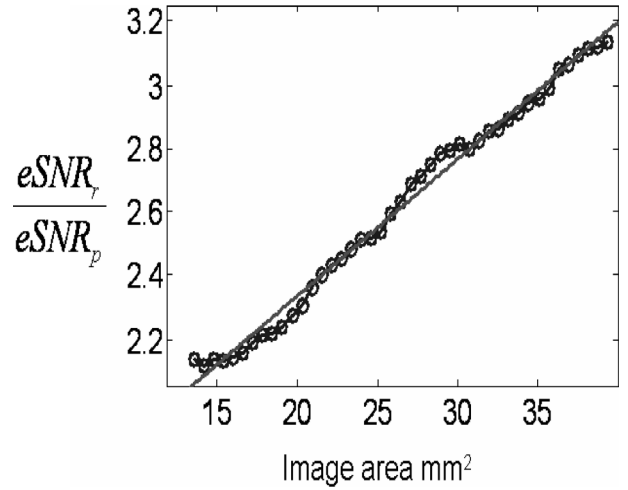


Fig. 3. The ratio  $eSNR_r/eSNR_p$  was measured experimentally as a function of the image area.

function  $\phi_h$ , and the shape is determined by the system bandwidth. Bandwidth can be quantified using the modulation transfer function (MTF) in two dimensions, given by the normalized discrete-time Fourier transform of  $h$  [16],

$$MTF(\mathbf{u}) = \frac{\sum_{\ell, m} h(\mathbf{x}, [\ell, m]) \exp(-i2\pi(\ell u_1/L + m u_2/M))}{\sum_{\ell, m} h(\mathbf{x}, [\ell, m])}.$$

From the discussion in Section II, frequencies  $\mathbf{u} = (u_1, u_2)$  can be temporal or spatial as required. The  $-20$  dB effective bandwidth of the system is defined from the area of MTF( $\mathbf{u}$ ) in the frequency plane  $(u_1, u_2)$  for which  $MTF > 0.1$ . Fig. 4(d) shows 2-D MTF( $\mathbf{u}$ ) = 0.1 contours for psfs originating at depths of 25, 40, and 64 mm, respectively.

Fig. 4(a) compares  $eSNR_p$  values before and after spatial matched filtering. Fig. 4(b) shows that predicted gain values,  $\gamma_{p(m)}$ , are comparable to measured values, and Fig. 4(c) shows the corresponding effective bandwidths at each depth. Two observations are immediately apparent from Figs. 4(a) and (b). Measurements are accurately predicted by (13), and the eSNR is enhanced more than 9 dB for the entire range following the SMF. The eSNR gain realized by matched filtering with  $h$  is derived from selectively suppressing noise in proportion to the system response. As predicted by (13), Figs. 4(b) and (c) show that the eSNR gain is lowest where the bandwidth is greatest.

We also predicted and measured  $eSNR_p$  gains using a wire target in a water tank and the Antares system. The objective was to compare conventional DRF with the SMF beamformer. We predicted  $eSNR_p$  values of 41.2, 43.5, and 41.1 dB for the SMF and 30.9, 31.0, and 30.2 dB for DRF, corresponding to the depths of 20, 40, and 45 mm, respectively. Thus, the predicted eSNR gains are 10.3, 12.5, and 10.9 dB. The measured values are, respectively, 9.2, 9.6, and 10.1 dB.

A previous study showed the eSNR could be further improved in the near field using the SMF if filtering is applied to echoes from each channel individually before

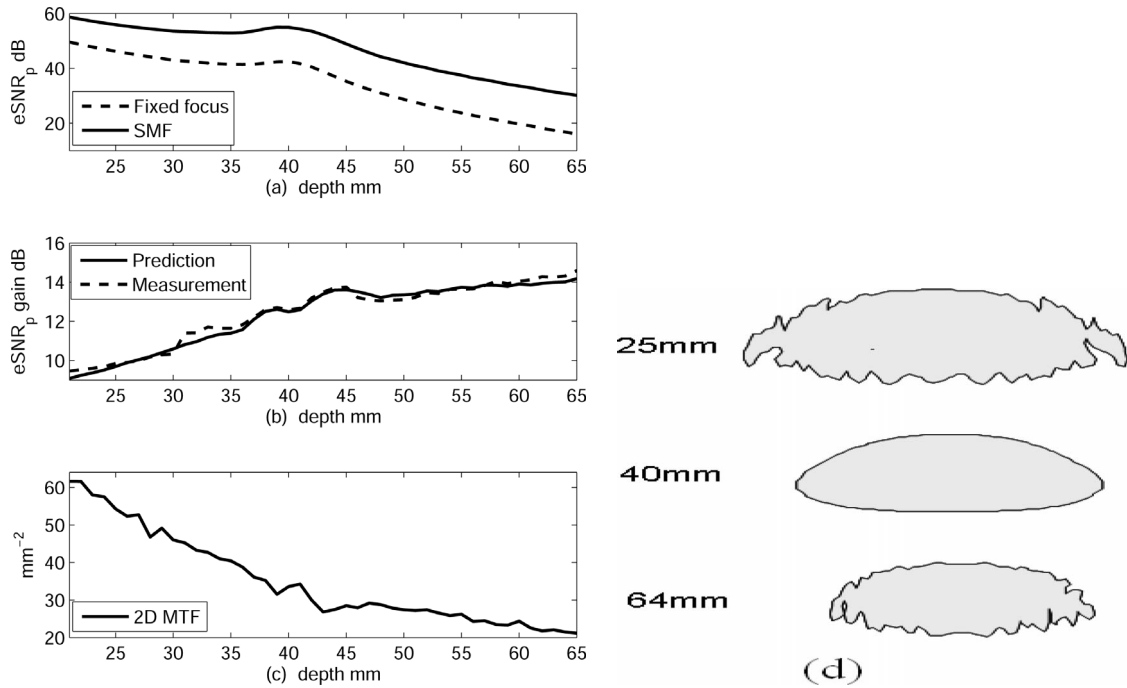


Fig. 4. (a) eSNR versus depth before ( $eSNR_p$ ) and after ( $eSNR_{p(m)}$ ) application of the spatial matched filter (SMF); (b) predicted and measured eSNR gains; (c)  $-20$  dB effective bandwidth versus depth as computed from 2-D MTF curves; (d) 2-D contours at MTF( $\mathbf{u}$ ) = 0.1 at depths of 25, 40, and 64 mm, respectively. The vertical and horizontal contour dimensions summarize the  $-20$  dB axial and lateral bandwidths.

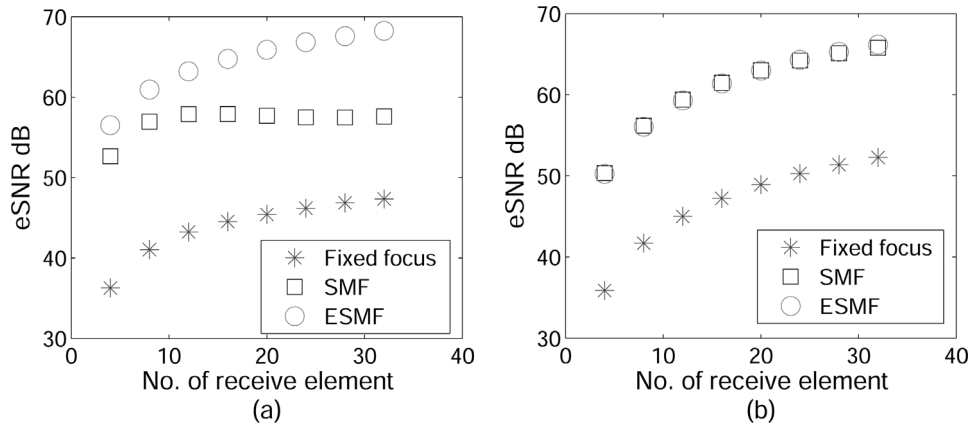


Fig. 5. The eSNR versus the number of elements before and after application of the spatial matched filter (SMF and ESMF) in the near field (a) and at focus (b).

summation (ESMF) [4]. Fig. 5 displays computed values of the eSNR for fixed focus, SMF, and ESMF beamformers as a function of receive channel number. Results at depths of 20 mm and 40 mm are given. The number of transmit channels is fixed at 32 for all beamforming methods. Three observations are apparent from Fig. 5. First, all beamformers increase the eSNR as the receive aperture increases. This makes sense since more of the scattered energy is detected. Second, in the near field [Fig. 5(a)], the relative gain in eSNR is greatest where the receive aperture, and therefore the 2-D signal bandwidth, are both relatively small. As the receive aperture and bandwidth grow, the eSNR increases but the gain in eSNR for filtering is reduced. Third, the ESMF beamformer increases the

eSNR more than the SMF in the near field [Fig. 5(a)], but there is no difference in eSNR between these methods at the focus [Fig. 5(b)]. In the focal region, all the elements have similar spatiotemporal responses. Eqs. (18) and (20) predicted equality when all the transducer elements have the same  $h_i$ . In the geometric near field, however,  $h_i$  varies significantly among the different receive channel elements. The greater coherence among receive-channel echo data filtered before summing leads to a higher eSNR.

### C. eSNR Gain for STF Beamformer

Field II simulations were also conducted to compare eSNRs using a DRF and an SMF combined with a STF,

as described in Section IV-B. A conventional Gabor pulse was transmitted for DRF and SMF results, while a 13-bit Barker code was transmitted for STF results, all with a carrier frequency of 10 MHz. Table I gives the results for each method at depths of 20, 40, and 60 mm. Coded pulse excitation increased the eSNR by about 11 dB.

## VI. DISCUSSION

Eq. (8) and Fig. 4 show that the eSNR varies significantly throughout the field for instruments with shift-varying impulse responses. Unfocused near-field regions of a fixed-focus aperture system contain greater eSNRs compared to the focal region and far field as shown in Fig. 4(a). There is also a greater effective bandwidth in the near field, suggesting the information content in the near field is greater than in the far field [5]. However, the greatest gain from the SMF occurs in the far field, which has the effect of equalizing the eSNR with depth. Narrow-band pulses gain more eSNRs than broadband pulses using an SMF. Transmitting a coded pulse appears to boost the eSNR uniformly with depth. However, pulse compression of beamformed signals produces geometric errors in the near field more than in the far field, thus generating range lobes [6]. Consequently contrast resolution can be affected.

The last form of (13) breaks down when comparing SMF and DRF methods because  $\phi_h$  in the numerator and denominator may not be the same. However, results can still be obtained numerically. Field II simulation results comparing the eSNR<sub>p</sub> for DRF and SMF beamformers and the eSNR gain are shown in Fig. 6. There are some minor differences, however; it seems that (13) can still be used to predict eSNR gains for many practical situations with good accuracy.

Eq. (23) gives the combined eSNR gain from an STF as the product of temporal coded excitation enhancement  $\gamma_{r(t)\Omega}$  and SMF enhancement  $\gamma_{r(m)\Omega}$ . If decoding is successful, the eSNR is increased by  $K$ . If it is incomplete, range sidelobes are generated that distort  $h(\mathbf{x}, \mathbf{t})/\phi_h$ . So the expression in (23) is an approximation. It is assumed that the pulse compression is complete.

We close by applying this eSNR analysis to another approach involving the correlation coefficient between two noisy signals,  $\mathbf{g}_1$  and  $\mathbf{g}_2$  [19]. The correlation coefficient  $\rho$  for a random medium in terms of (3) is

$$\begin{aligned} \rho &= \frac{\mathcal{E} \left\{ \sum_{\ell, m} g_1[\ell, m] g_2[\ell, m] \right\}}{\mathcal{E} \left\{ \sqrt{\sum_{\ell, m} g_1^2[\ell, m] \sum_{\ell, m} g_2^2[\ell, m]} \right\}} \\ &= \frac{\sigma_f^2 \sum_{\ell, m} \int_{\Omega} d\mathbf{x} h^2(\mathbf{x}, [\ell, m])}{\sigma_f^2 \sum_{\ell, m} \int_{\Omega} d\mathbf{x} h^2(\mathbf{x}, [\ell, m]) + \sigma_e^2 LM} \\ &= \frac{\text{eSNR}_r}{\text{eSNR}_r + 1}, \end{aligned} \quad (24)$$

TABLE I

ESNR GAIN IN DECIBELS VERSUS DEPTH FOR DRF, SMF, AND STF BEAMFORMERS.

Depth (mm)	DRF	SMF	STF
20	49.4	58.6	69.4
40	42.6	55.0	66.0
60	19.5	32.9	44.0

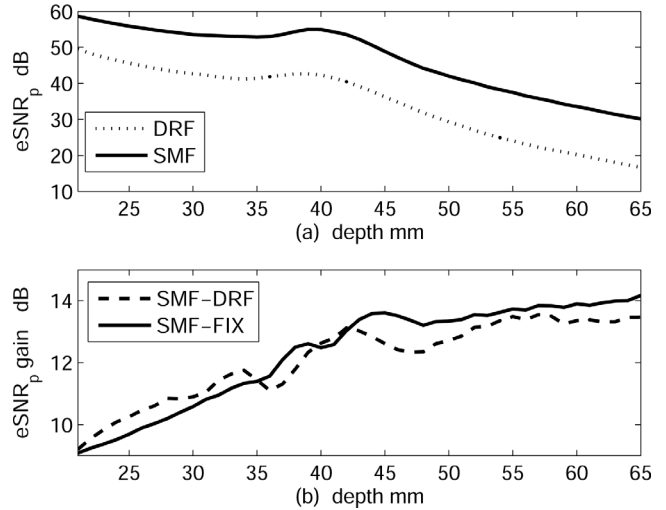


Fig. 6. (a) eSNR<sub>p</sub> comparisons for DRF and SMF beamformers versus depth; (b) corresponding eSNR<sub>p</sub> gain versus depth.

and therefore

$$\text{eSNR}_r = \frac{\rho}{1 - \rho}. \quad (25)$$

Eq. (6) expresses the eSNR<sub>r</sub> in terms of the system impulse response, object characteristics, and noise. Eq. (25) describes the eSNR<sub>r</sub> experimentally, based on statistical correlations of the data. It builds intuition for the eSNR in situations where decorrelation is a noise source [20], such as speckle tracking, phase aberration correction, and elastography. Together experimental results can be interpreted in terms of system and object properties.

## VII. CONCLUSIONS

In this paper, we propose an eSNR definition for pulse-echo systems that adapt to the effects of shift-varying impulse responses, spatiotemporal coding, and various beamformers. Measurement techniques using point targets or random scattering media can be interrelated for a broad range of experimental conditions. Tradeoffs between spatial resolution and depth of field are contained in this eSNR analysis. Closed-form expressions were found to predict the measured eSNR gains using SMF and STF beamformers, and the gains are significant—on the order of 10 dB for an SMF in the near field.

## REFERENCES

- [1] K. E. Thomenius, "Evolution of ultrasound beamformers," in *Proc. IEEE Ultrason. Symp.*, 1996, pp. 1615–1622.
- [2] M. Fatemi and A. C. Kak, "Ultrasonic B-scan imaging: Theory of image formation and a technique for restoration," *Ultrason. Imag.*, vol. 2, pp. 1–47, 1980.
- [3] S. Freeman, P.-C. Li, and M O'Donnell, "Retrospective dynamic transmit focusing," *Ultrason. Imag.*, vol. 17, pp. 173–196, 1995.
- [4] K.-S. Kim, J. Liu, and M. F. Insana, "Efficient array beam forming by spatial filtering for ultrasonic B-mode imaging," *J. Acoust. Soc. Amer.*, vol. 120, pp. 852–861, 2006.
- [5] R. J. Zemp, M. D. Parry, C. K. Abbey, and M. F. Insana, "Detection performance theory for ultrasound imaging systems," *IEEE Trans. Instrum. Meas.*, vol. 24, pp. 300–310, 2005.
- [6] J. Liu, K.-S. Kim, and M. F. Insana, "Beamforming using spatio-temporal filtering," in *Proc. IEEE Ultrason. Symp.*, 2005, pp. 1216–1219.
- [7] H. L. Van Trees, *Detection, Estimation, and Modulation Theory, Part I*. New York: Wiley, 1968.
- [8] R. N. McDonough and A. D. Whalen, *Detection of Signal in Noise*. 2nd ed. San Diego: Academic Press, 1995.
- [9] J. A. Jensen and N. B. Svendsen, "Calculation of pressure fields from arbitrarily shaped, apodized, and excited ultrasound transducers," *IEEE Trans. Ultrason., Ferroelect., Freq. Contr.*, vol. 39, pp. 262–267, 1992.
- [10] G. E. Tupolme, "Generation of acoustic pulses by baffled plane pistons," *Mathematika*, vol. 16, pp. 209–224, 1969.
- [11] P. R. Stepanishen, "Acoustic transients from planar axisymmetric vibrators using the impulse response approach," *J. Acoust. Soc. Amer.*, vol. 70, pp. 1176–1181, 1981.
- [12] R. J. Zemp, C. K. Abbey, and M. F. Insana, "Linear system models for ultrasonic imaging: Application to signal statistics," *IEEE Trans. Ultrason., Ferroelect., Freq. Contr.*, vol. 50, pp. 642–654, 2003.
- [13] J. M. Thijssen, B. J. Oosterveld, and R. F. Wagner, "Gray level transforms and lesion detectability in echographic images," *Ultrason. Imag.*, vol. 10, pp. 171–195, 1988.
- [14] J. A. Jensen and P. Gori, "Improved accuracy in the estimation of blood velocity vectors using matched filtering," in *Proc. IEEE Ultrason. Symp.*, 2000, pp. 1507–1511.
- [15] J. Liu and M. F. Insana, "Coded pulse excitation for ultrasonic strain imaging," *IEEE Trans. Ultrason., Ferroelect., Freq. Contr.*, vol. 52, pp. 231–240, 2005.
- [16] E. C. Farnett and G. H. Stevens, "Pulse compression radar," in *Radar Handbook*. 2nd ed. M. Skolnik, Ed. New York: McGraw-Hill, 1990.
- [17] J. Liu, C. K. Abbey, and M. F. Insana, "Linear approach to axial resolution in elasticity imaging," *IEEE Trans. Ultrason., Ferroelect., Freq. Contr.*, vol. 51, pp. 716–725, 2004.
- [18] R. F. Wagner, S. W. Smith, J. M. Sandrik, and H. Lopez, "Statistics of speckle in ultrasound B-scans," *IEEE Trans. Sonics Ultrason.*, vol. 30, pp. 156–163, 1983.
- [19] B. H. Friemel, L. N. Bohs, and G. E. Trahey, "Relative performance of two-dimensional speckle-tracking techniques: Normalized correlation, non-normalized correlation and sum-absolute-difference," in *Proc. IEEE Ultrason. Symp.*, 1995, pp. 1481–1484.
- [20] W. F. Walker, "The significance of correlation in ultrasound signal processing," *Proc. SPIE*, vol. 4325, pp. 159–171, 2001.



**Jie Liu** obtained her Ph.D. degree in biomedical engineering at Tsinghua University, Beijing, China, in 2001. Following her graduate work, Dr. Liu moved to the University of Washington, Seattle, WA, as a Senior Research Fellow in the Bioengineering Department working on medical image registration. From 2002 to 2004, she was a postdoctoral researcher in the Biomedical Engineering Department at the University of California, Davis, CA, where she conducted coded-excitation approaches for B-mode, elasticity, and Doppler estimation. From 2004–2006, she was a research assistant professor in the Bioengineering Department at the University of Illinois at Urbana-Champaign. She is currently working at GE Healthcare as an Ultrasound Systems Engineer. Her research interests include developing advanced scientific theories, methods, and research techniques in medical ultrasonic imaging system and evaluating their performances in terms of diagnostic tasks.



**Kang-Sik Kim** earned his B.S. and M.S. degrees in electronic engineering from Sogang University, Seoul, South Korea, in 1999 and 2001, respectively. He obtained his Ph.D. degree in electronic engineering at the Center for Medical Solutions Research, Sogang University, Seoul, South Korea, in 2005. He was a postdoctoral research associate in the Bioengineering Department, University of Illinois at Urbana-Champaign, from 2005 to 2006. His research interests include signal processing and system design for medical ultrasound imaging system.



**Michael F. Insana** (M'85) received his Ph.D. degree in medical physics from the University of Wisconsin-Madison in 1983. His dissertation topic was acoustic scattering and absorption in biological tissues. He was a research physicist at the FDA from 1984–1987, where he developed methods for describing tissue microstructure from the statistical properties of echo signals. From 1987–1999 he was with the Department of Radiology at the University of Kansas Medical Center. There he directed an imaging research lab

that applied ultrasonic imaging to the evaluation of progressive renal failure and breast cancer. Between 1999 and 2004, Mike was Professor of Biomedical Engineering at the University of California, Davis, where he directed the graduate program. He is currently Professor of Bioengineering and ECE at the University of Illinois at Urbana-Champaign. His research includes the development of novel ultrasonic instrumentation and methods for imaging soft tissue microstructure, viscoelasticity, and blood flow. The goal is to understand basic mechanisms of tumor formation and responses to therapy. He is also interested in the principles of imaging system design and performance evaluation, and signal processing, detection, and estimation. He is a member of the Acoustical Society of America, Senior Member of the IEEE, Fellow of the Institute of Physics, Fellow of the American Institute of Medical and Biological Engineering, and Associate Editor for *IEEE Transactions on Medical Imaging*.